Variation of Landau level splitting in the Fermi level controlled Dirac metals (Eu, Gd)MnBi$_2$

H. Sakai [ORCID],[1,*] K. Nakagawa,[1] K. Tsuruda,[1] J. Shiogai [ORCID],[2,†] K. Akiba,[3,‡] M. Tokunaga [ORCID],[3] S. Kimura,[2] S. Awaji [ORCID],[2] A. Tsukazaki [ORCID],[2] H. Murakawa,[1] and N. Hanasaki [ORCID][1,4]

[1]*Department of Physics, Osaka University, Toyonaka, Osaka 560-0043, Japan*
[2]*Institute for Materials Research, Tohoku University, Sendai 980-8577, Japan*
[3]*The Institute for Solid State Physics, The University of Tokyo, Kashiwa, Chiba 277-8581, Japan*
[4]*Spintronics Research Network Division, Institute for Open and Transdisciplinary Research Initiatives, Osaka University, Suita, Osaka 565-0871, Japan*

We have experimentally studied the Landau levels near the quantum limit in the magnetic Dirac material (Eu, Gd)MnBi$_2$. In this series of materials, the Fermi level is systematically controlled by substituting Eu^{2+} with Gd^{3+} while keeping high mobility. We measured the Shubnikov–de Haas (SdH) oscillation for a single crystal with the lowest hole concentration at tilted magnetic fields up to 20–50 T and clarified the dependence of the splitting of the Landau levels $N \geqslant 1$ on the ratio of Zeeman energy to cyclotron energy. In the low-field antiferromagnetic phase, the splitting is well explained by the (Zeeman) spin splitting, from which we have found that the effective g factor of the Dirac fermion depends significantly on the Fermi energy. In the high-field antiferromagnetic phase, on the other hand, the SdH oscillation was found to change in a complex manner as a function of the tilt angle of the field, implying the lifting of the valley degeneracy as well as the spin degeneracy.

I. INTRODUCTION

Magnetic materials hosting relativistic quasiparticles, called Dirac-Weyl magnets, have attracted much attention not only in fundamental physics but also in potential applications owing to their unconventional transport phenomena [1,2]. In Weyl magnets, for instance, the Weyl points (i.e., nondegenerate linearly crossing bands) formed by the peculiar magnetic and/or lattice structures work as a source of the Berry phase, leading to giant anomalous Hall and Nernst effects [3–12] and magneto-optical responses [13,14]. Another important feature of the relativistic quasiparticle is ultrahigh mobility due to the suppression of backscattering, which may enable new spintronic functions when coupled with the magnetism. However, Dirac-Weyl magnets rarely exhibit high mobility probably due to the influence from many trivial carriers.

In contrast to this, AMnX_2 (A = alkaline and rare-earth ions; X = Sb, Bi) is a promising series of materials for achieving both high mobility and magnetic order [15–33]. Since its crystal structure consists of the alternate stacking of two-dimensional (2D) Dirac fermion layers (X^- square net) [34] and magnetic block layers (A^{2+}-Mn^{2+}-X^{3-}) [Fig. 1(a)], the high-mobility transport of the Dirac fermion is controllable by modifying the spatially separated block layer [35]. In fact, in EuMnBi$_2$ (A = Eu, X = Bi), the quantum transport phenomena significantly vary as a function of the field-tunable antiferromagnetic (AFM) order of the Eu layer; the large magnetoresistance effect manifests itself when the Eu spins flop by applying an external field [25,26], accompanied by a marked change in quantum oscillation [26]. Specifically, the spin splitting of Landau levels (LLs) depends on the AFM order of the Eu layer, which is explained by the strong exchange interaction between the Dirac fermion and the Eu spin [36].

The block layer for this material also works as charge reservoir for the Dirac fermion layer. Partial substitution of Eu^{2+} with Gd^{3+} reduces the hole concentration in EuMnBi$_2$, which is unintentionally hole doped, and even makes the crystal n type across the charge neutral point. Consequently, the Seebeck and Nernst effects were widely and systematically tuned by Gd concentration in (Eu, Gd)MnBi$_2$ [37]. The variation in LLs should also be interesting when the Fermi level approaches the Dirac point; the extreme quantum limit can be achieved at strong magnetic fields. In the LLs near the Dirac point, the simple single-particle picture may break down due to the many-body interaction and lift the sublattice (valley) degeneracy, as intensively investigated for graphene [38–40]. For EuMnBi$_2$, only the LLs $N \geqslant 2$ were observed in the AFM phases (below ∼20 T), where the quantum oscillation is enhanced due to the two-dimensional confinement [26,36]. Thus the low-energy LLs near the Dirac point have not been uncovered in this material.

In this paper, we performed high-field transport measurements on (Eu, Gd)MnBi$_2$ single crystals with reduced hole concentration to clarify the detailed features of low-energy LLs including $N = 1$. In particular, we measured the Shubnikov–de Haas (SdH) oscillation by changing the tilt angle of the field, i.e., the Zeeman-energy-to-cyclotron-energy ratio. We have found that the spin splitting is dominant in the LLs $N \geqslant 3$ observed in the low-field AFM phase and

---

*Corresponding author: sakai@phys.sci.osaka-u.ac.jp

†Present address: Department of Physics, Osaka University, Toyonaka, Osaka 560-0043, Japan.

‡Present address: Graduate School of Natural Science and Technology, Okayama University, Okayama 700-8530, Japan.
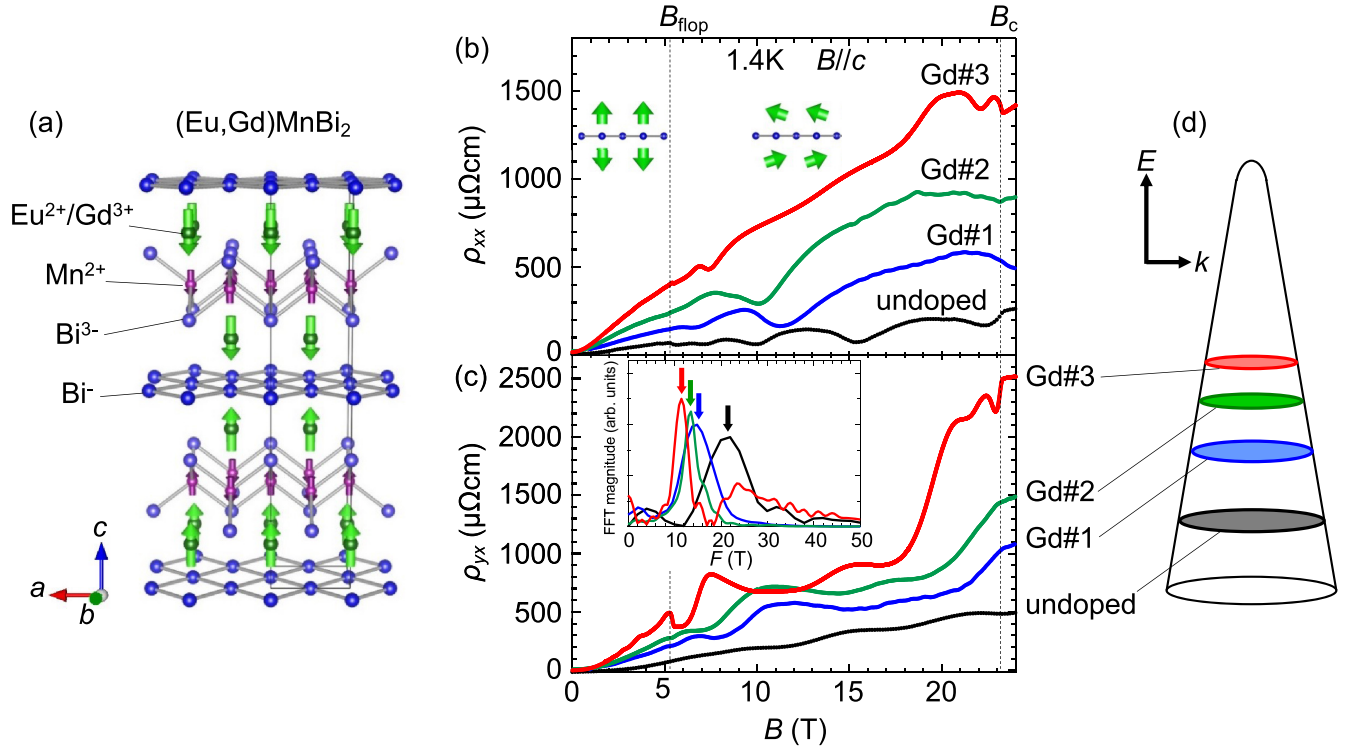
FIG. 1. (a) Crystal structure of (Eu, Gd)MnBi$_2$ showing the antiferromagnetic (AFM) order at 0 T (low-field AFM order) [42,43]. (b) and (c) Field dependences of in-plane resistivity ρ_{xx} (b) and Hall resistivity ρ_{yx} (c) at 1.4 K ($B \parallel c$) for EuMnBi$_2$ (undoped) and Gd-doped EuMnBi$_2$ (samples Gd#1–Gd#3). B_{flop} and B_c denote the transition fields to the high-field AFM and forced ferromagnetic phases, respectively. Insets in (b): Schematic illustrations of the low-field (left) and high-field (right) AFM orders of the Eu layer. Inset in (c): Fast Fourier transform (FFT) of the oscillatory component of ρ_{yx} below B_{flop}. The peak position corresponds to the frequency of SdH oscillation. (d) Schematic illustration of E_F shift as a function of Gd substitution in the 2D massive Dirac cone for (Eu, Gd)MnBi$_2$.

that the effective g factor is enhanced as the Fermi energy approaches the Dirac point. On the other hand, in the LLs $N = 1$ and 2 appearing in the high-field AFM phase, additional splitting other than the spin origin was clearly observed. As a result, the SdH oscillation shows a much more complicated dependence on the tilt angle of the field. We shall discuss the origin in terms of the lifting of spin and valley degeneracy.

II. EXPERIMENT

Single crystals of (Eu, Gd)MnBi$_2$ were grown by a Bi self-flux method [37]. High-purity ingots of Eu (99.9%), Gd (99.9%), Mn (99.9%), and Bi (99.999%) were mixed in the ratio Eu : Gd : Mn : Bi = $1 - x : x : 1 : 9$ and put into an alumina crucible in an argon-filled glove box ($x = 0$, 0.005, 0.0075, and 0.01) The crucible was sealed in an evacuated quartz tube and heated at 1000 °C for 10 h, followed by slow cooling to 350 °C at a rate of ~ 2 °C/h, where the excess Bi flux was decanted using a centrifuge. The powder x-ray diffraction at room temperature indicates that the crystal structure of the obtained single crystals is tetragonal ($I4/mmm$) and the lattice constants are almost unchanged irrespective of the nominal Gd concentration. Since the Gd concentration in the obtained crystals is too low to be precisely determined by the energy-dispersive x-ray analysis, the variation in E_F among the samples was determined by their transport prop-

erties, i.e., SdH oscillation and the Hall effect, as shown below. We thereby label the Gd-doped samples as samples Gd#1–#Gd3 in order of increasing E_F [from low to high; see Fig. 1(d)], as was adopted in Ref. [37].

In-plane resistivity ρ_{xx} and Hall resistivity ρ_{yx} were measured by a conventional five-terminal method with electrodes formed by room-temperature curing silver paste. For precise measurements, we adopted the lock-in technique at 20–150 Hz with an ac excitation of 1–5 mA. The measurements up to 24 T at 1.4 K were performed (for sample Gd#3) with the 25-T cryogen-free superconducting magnet (25T-CSM) at the High Field Laboratory for Superconducting Materials in the Institute for Materials Research, Tohoku University [41]. The field direction was controllable by using a sample probe equipped with a rotating stage, where the tilt angle of the field was determined by a Hall sensor attached on the sample stage. The measurements up to 55 T at 1.4 K were performed (for the undoped sample, sample Gd#1, and sample Gd#2) by using a nondestructive pulsed magnet at the International Mega-Gauss Science Laboratory at the Institute for Solid State Physics.

III. RESULTS AND DISCUSSION

Figures 1(b) and 1(c) show the field dependences of ρ_{xx} and ρ_{yx} for (Eu, Gd)MnBi$_2$ single crystals at 1.4 K for the field parallel to the c axis ($B \parallel c$), respectively. At zero field,

Eu spins order ferromagnetically within the *ab* plane and align along the *c* axis in the AFM sequence of up-up-down-down [low-field AFM phase shown in Fig. 1(a)] [26,42,43]. As schematically shown in the insets in Fig. 1(b), the AFM order of Eu spins can be controlled by applying the external magnetic field parallel to the *c* axis. Above B_{flop}, the direction of Eu spins flops from the *c* axis to the *ab* plane (high-field AFM phase), while all Eu spins are aligned ferromagnetically above B_c (forced ferromagnetic phase). The values of B_{flop} and B_c are almost independent of Gd concentration, which can be determined by the weak anomalies (i.e., a small kink or jump) in ρ_{xx} and ρ_{yx} [vertical dotted lines in Figs. 1(b) and 1(c)]. As the Gd concentration increases, the slope of ρ_{yx} with respect to field increases [Fig. 1(c)], which evidences that the hole carriers existing in the undoped sample are reduced by Gd substitution and the Fermi energy E_F moves toward the charge-neutral point [Fig. 1(d)]. Interestingly, the field dependence of ρ_{xx} also varies systematically as a function of Gd substitution. Apart from the oscillatory component arising from the SdH oscillation (*vide infra*), the background of ρ_{xx} is nearly linear with field, the slope of which progressively increases with Gd concentration. For instance, $\rho(20\ \text{T})/\rho(0\ \text{T}) = 1800\%$ for the undoped sample, while $\rho(20\ \text{T})/\rho(0\ \text{T}) = 8300\%$ for sample Gd#3. Since the carrier mobility remains almost unchanged among the samples [37], the carrier compensation due to electron doping may play a role in such an enhancement in the magnetoresistance effect.

All the ρ_{xx} and ρ_{yx} data shown in Fig. 1 exhibit marked SdH oscillations, which reflect the high mobility of the Dirac fermion even in the Gd-substituted crystals. By analyzing the SdH oscillation in detail, we are able to obtain more quantitative information on the variation in the Dirac fermion as a function of Gd substitution. The inset in Fig. 1(c) shows the fast Fourier transform of the oscillation component of ρ_{yx}, where the frequency of SdH oscillation, the extremal cross section of the quasi-2D cylindrical Fermi surface, systematically decreases with increasing Gd substitution. For sample Gd#3, the frequency decreases to approximately half of that for the undoped sample. The fine structures of SdH oscillation, such as splitting of the peak, are also important to reveal the microscopic features of the system, since they correspond to the LL splitting caused by the Zeeman interaction and/or many-body electron-electron interaction. Below, to study the details of SdH oscillation, we analyze longitudinal conductivity $\sigma_{xx} = \rho_{xx}/(\rho_{xx}^2 + \rho_{yx}^2)$, which directly reflects the density of states of LLs in the conventional quantum Hall systems.

Figure 2(a) presents σ_{xx} versus $1/B$ at 1.4 K for the undoped sample, sample Gd#1, and sample Gd#3. Note here that the dip in σ_{xx} corresponds to the energy gap between the LLs (i.e., the quantum Hall gap). For the undoped sample, the LLs $N = 1$, 2, and 3 appear in the high-field AFM phase ($1/B_c < 1/B < 1/B_{\text{flop}}$), although the LL $N = 1$ is terminated in the middle at B_c. For sample Gd#3 with the lowest hole concentration, on the other hand, almost the entire LL $N = 1$ is formed at $1/B_c < 1/B$. To clarify the split structure, we here take the second derivative of σ_{xx} with respect to the field for sample Gd#3 as shown in Fig. 2(b). In the low-field AFM phase ($1/B_{\text{flop}} < 1/B$), the LLs $N = 3$, 4, and 5 are clearly
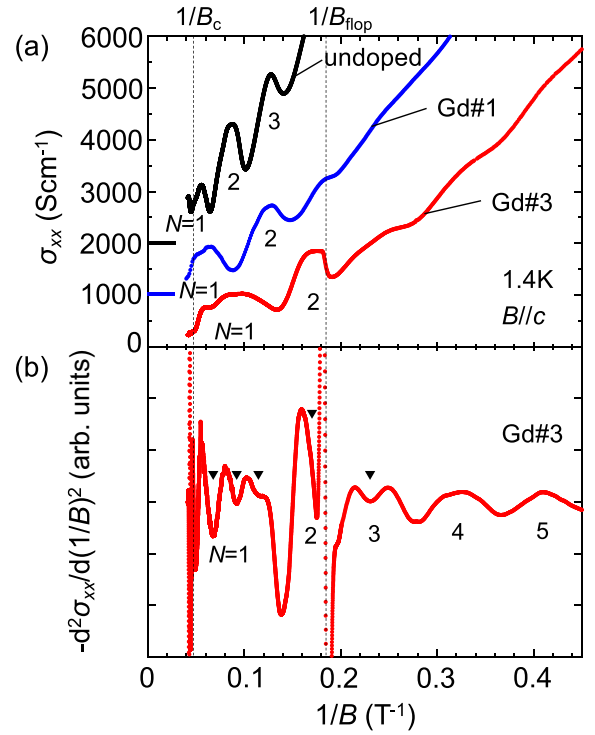
FIG. 2. (a) In-plane conductivity σ_{xx} vs $1/B$ at 1.4 K with $B \parallel c$ for the undoped and Gd-doped crystals. Each profile is shifted vertically for clarity. N indicates the Landau index. (b) $-d^2\sigma_{xx}/d(1/B)^2$ vs $1/B$ for sample Gd#3 [44]. The inverted triangles denote the splitting of the Landau levels.

identified, where the LL $N = 3$ exhibits clear splitting. The splitting is more conspicuous in the high-field AFM phase. Noting that the deep dip at $1/B = 0.12\ \text{T}^{-1}$ corresponds to the energy gap between $N = 1$ and $N = 2$, the LL $N = 1$ apparently splits into four as denoted by the inverted triangles. This suggests the lifting of both spin and valley degeneracy (as detailed later in Fig. 4).

To reveal the origin of the LL splitting, we studied the variation of σ_{xx} when the field is tilted from the *c* axis to the *ab* plane. For a 2D system, the ratio of Zeeman energy E_Z to cyclotron energy E_c varies depending on the tilt angle θ of the field [36,45–47]:

$$E_Z/E_c = \frac{g^* m_c}{2m_0 \cos\theta}. \qquad (1)$$

This results from the fact that $E_Z = g^* \mu_B B$ is proportional to the total field B while $E_c = e\hbar B_\perp/m_c$ is proportional to the field component perpendicular to the 2D plane ($B_\perp = B\cos\theta$), where g^* is the effective *g* factor, m_c is the cyclotron mass, and m_0 is the bare electron mass. Consequently, by analyzing the θ dependence of the SdH oscillation, we can quantitatively estimate the microscopic parameters of 2D electrons, such as $g^* m_c$. Note here that since the energy spacing of Landau levels for a 2D Dirac fermion is not uniform (i.e., E_c is dependent on N), we need to effectively define $E_c \equiv e\hbar B_\perp/m_c$ by using a semiclassical expression of the cyclotron mass $m_c = E_F/v_F^2$ with v_F being the Fermi velocity [48,49]. With this definition, E_Z/E_c indicates the magnitude of the Zeeman spin splitting in the SdH oscillation [36], as
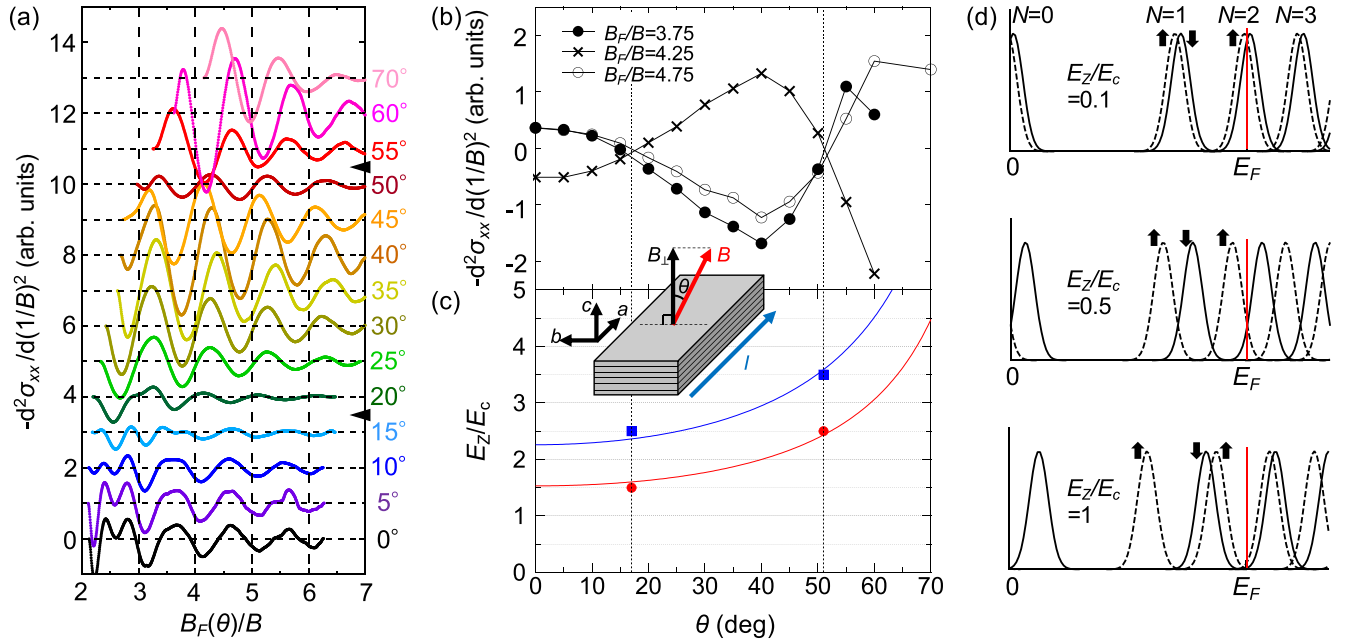
FIG. 3. (a) $-d^2\sigma_{xx}/d(1/B)^2$ vs $B_F(\theta)/B$ in the low-field AFM phase ($1/B_{\mathrm{flop}} < 1/B$) at various tilt angles θ for sample Gd#3 (1.4 K). Each profile is shifted vertically. The phase of the SdH oscillation is inverted around the arrowheads shown on the right axis. (b) and (c) θ dependences of the peak ($B_F/B = 3.75$ and 4.75) and dip ($B_F/B = 4.25$) values of $-d^2\sigma_{xx}/d(1/B)^2$ (b) and the Zeeman-energy-to-cyclotron-energy ratio (E_Z/E_c) (c). Vertical dotted lines denote the θ values where the phase of SdH oscillation is inverted. In (c), the red (blue) solid curve denotes $\frac{g^* m_c}{2m_0 \cos\theta}$ for $g^* m_c/m_0 = 3.1$ (4.5), where the phase inversion corresponds to $E_Z/E_c = 1.5$ and 2.5 ($E_Z/E_c = 2.5$ and 3.5). Inset: Geometry of the transport measurements in a tilted magnetic field, where θ is the angle between the field and the c axis. (d) Spin-split Landau levels ($N = 0$–3) of a 2D massless Dirac fermion at $B_F(\theta)/B = 2$ as a function of energy, where the solid (dashed) curve represents the spin-down (spin-up) Landau level. As E_Z/E_c increases as a function of θ, the density of states at E_F changes as follows: A peak for $E_Z/E_c = 0.1$ (top panel), a node for $E_Z/E_c = 0.5$ (middle panel), and a dip for $E_Z/E_c = 1$ (bottom panel). For details of the calculation, see Supplemental Material, Fig. S4 [50].

in the case for a normal 2D electron gas (for details, see Supplemental Material, Fig. S4 [50]). Below, we analyze the LL splitting for each AFM phase in detail and compare the results for sample Gd#3 with those for the undoped sample to see the dependence on E_F.

We first focus on the low-field AFM phase. Figure 3(a) displays $-d^2\sigma_{xx}/d(1/B)^2$ versus $B_F(\theta)/B$ for sample Gd#3 at 1.4 K for various θ, where the field is tilted from the c axis toward the b axis and the current is applied along the a axis [inset of Fig. 3(c)]. In principle, σ_{xx} in a tilted field is calculated as $\sigma_{xx} = \frac{\rho_{xx}}{\rho_{xx}^2 + \rho_{yx}^2}(1 + \frac{\rho_{zx}^2 \rho_{xx}}{(\rho_{xx}^2 + \rho_{yx}^2)\rho_{zz}})^{-1}$. However, from the previous study on the undoped sample [36], it is known that the factor $\frac{\rho_{zx}^2 \rho_{xx}}{(\rho_{xx}^2 + \rho_{yx}^2)\rho_{zz}}$ is so small ($\ll 1$) for $\theta \leqslant 70°$ that σ_{xx} is safely approximated as $\sigma_{xx} = \frac{\rho_{xx}}{\rho_{xx}^2 + \rho_{yx}^2}$ [51]. $B_F(\theta)$ is the SdH frequency for each θ, deduced from the fast Fourier transform. Reflecting the quasi-two-dimensional Fermi surface, $B_F(\theta)$ is proportional to $1/\cos\theta$ up to $\theta = 60°$, although it significantly deviates downward above $\theta = 70°$ presumably owing to the warping of the cylindrical Fermi surface (see Fig. S1 for details [50]). To clarify the θ dependence of LL splitting, it is useful to plot the SdH oscillations as a function of $B_F(\theta)/B$, which is the filling factor normalized by the spin and valley degeneracy factor [36,52], i.e., $B_F(\theta)/B = N + 1/2 - \gamma$, where N is the Landau index and γ is the phase factor expressed as $\gamma = 1/2 - \phi_B/2\pi$ with ϕ_B being the Berry

phase [53,54]. The deep minima of the oscillation correspond to the energy gap between the LLs. Although these minima should be located at $N + 1/2$ for the Dirac fermion exhibiting the Berry phase of π ($\phi_B = \pi$), their positions are found to be around $N + 1/4$. This slight phase shift might arise from the fact that the Fermi surface is not exactly two dimensional. At $\theta = 0°$, the LLs $N = 3$–6 are observed, where a clear split structure is discernible for $N = 3$, as explained in Fig. 2(b). Noteworthy is that the amplitude and phase of the SdH oscillation systematically vary as θ increases from 0°. At first, the amplitude monotonically decreases and reaches the minimum at $\theta \sim 15°$. However, it begins to increase above 20°, where the phase of the oscillation is inverted (i.e., the peaks are located around $N + 1/4$). The amplitude reaches the maximum at $\theta \sim 40°$ and then decreases, reaching the minimum at $\theta = 50°$. Above 50°, the phase of oscillation is again inverted.

Such variation of SdH oscillation as a function of θ is well explained by spin splitting of LLs, as schematically shown in Fig. 3(d). The LLs slightly split for $E_Z/E_c = 0.1$ (top panel). As E_Z/E_c increases to 0.5, the splitting evolves, and the amplitude of the SdH oscillation becomes minimum (middle panel). A further increase in E_Z/E_c up to 1 leads to crossing of the neighboring LLs with opposite spins, which results in the enhanced SdH oscillation with an inverted phase (bottom panel). For each integer change in E_Z/E_c, the SdH oscillation
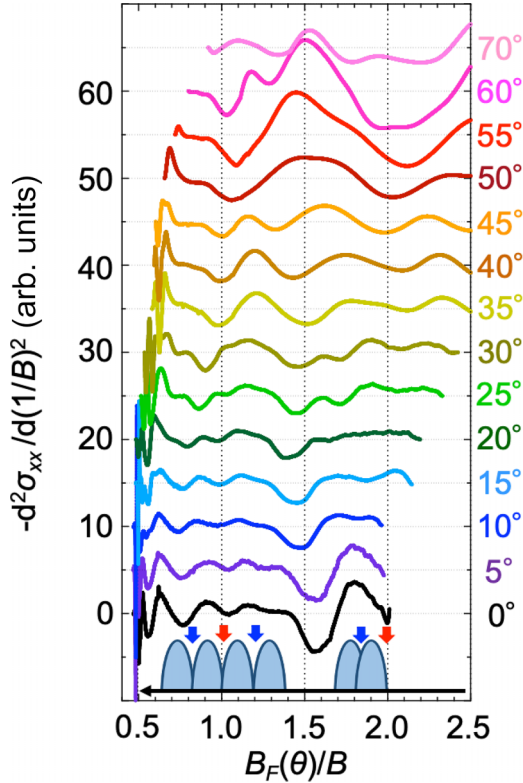
FIG. 4. $-d^2\sigma_{xx}/d(1/B)^2$ vs B_F/B in the high-field AFM phase ($1/B < 1/B_{\text{flop}}$) at various tilt angles θ for sample Gd#3 (1.4 K) [44]. Each profile is shifted vertically. A schematic of the Landau levels is shown at the bottom, where red (blue) arrows indicate the splitting at $B_F/B = N$ ($N \pm 1/4$).

repeats this variation. Note here that for the LLs with large N ($N \geqslant 4$), the spin splitting with respect to B is small, which makes it difficult to observe a clear splitting structure (see Fig. S4 for a calculation of the SdH oscillation of the spin-split LLs [50]).

To quantitatively clarify such θ dependence of the SdH oscillation, we plot the peak and dip values of $-d^2\sigma_{xx}/d(1/B)^2$ versus θ [Fig. 3(b)]. There, $B_F/B = 4.25$ corresponds to the dip in the oscillation at $\theta = 0°$, while $B_F/B = 3.75$ and 4.75 correspond to the peak at $\theta = 0°$. With increasing θ, the peak and dip values are first inverted at $\sim 17°$, followed by the second inversion at $\sim 52°$. Since the phase inversion of SdH oscillation corresponds to half-integer values of E_Z/E_c ($= 0.5, 1.5, 2.5, \ldots$), the observed θ dependence means that E_Z/E_c passes through the half-integer value twice from $\theta = 0°$ to $\theta = 70°$. By adjusting the g^*m_c value in Eq. (1), we have found that two cases well reproduce the experimental θ dependence [Fig. 3(c)]: (i) $E_Z/E_c = 1.5$ ($\theta = 17°$) and $E_Z/E_c = 2.5$ ($\theta = 51°$), displayed in red, and (ii) $E_Z/E_c = 2.5$ ($\theta = 17°$) and $E_Z/E_c = 3.5$ ($\theta = 51°$), displayed in blue. Since the value of m_c/m_0 is independently estimated to be 0.080(3) from the temperature dependence of the SdH oscillation at $\theta = 0°$ based on the standard Lifshitz-Kosevich formula (Fig. S2 [50]), we obtain $g^* = 37 \pm 2$ for case (i) and $g^* = 54 \pm 2$ for case (ii).

Also for the undoped sample, a similar phase inversion of the SdH oscillation was observed in the low-field AFM phase when the field is tilted [36]. However, the phase

inversion occurs only once at $\theta = 18°$ (see Fig. S3 for details [50]), which results in $g^* \sim 10$ [55]. Therefore the effective g factor is larger for sample Gd#3 than for the undoped sample; it likely increases as E_F approaches the charge-neutral point. The E_F dependence of the effective g factor is roughly explained by the theoretical expression obtained by the $k \cdot p$ theory in the presence of spin-orbit interaction [56]; it has a leading term $\propto 1/(\Delta E + |E_F|)$, where ΔE is the energy gap of the massive Dirac band. However, the enhancement of the effective g factor is estimated to be ~ 20–30% for sample Gd#3 when we adopt the results of band calculation, i.e., $\Delta E \sim 50$ meV and $E_F \sim -40$ meV for the undoped sample while $E_F \sim -25$ meV for sample Gd#3. The origin of such a quantitative difference remains unclear but might be relevant to the many-body effect.

Several other mechanisms have been reported to explain the variation of SdH oscillations as a function of tilting the field. In 3D Weyl semimetals, for instance, the phase may be affected by the change in the extremal orbits of the anisotropic Fermi surface [57]. It is also reported that the band dispersion may be modified by a magnetic field tilted away from the high-symmetry direction [58,59]. However, in both cases, the SdH phase exhibits various values depending on the field direction while the SdH amplitude remains unchanged. These features are different from what was observed in (Eu, Gd)MnBi$_2$.

Next, to show the details of LL splitting in the high-field AFM, we plotted $-d^2\sigma_{xx}/d(1/B)^2$ versus $B_F(\theta)/B$ at $1/B < 1/B_{\text{flop}}$ for various θ in Fig. 4. There, we adopt $B_F(\theta)$ obtained in the low-field AFM phase. (For the undoped sample, the change in B_F between the high-field and low-field AFM phases is less than 3%.) For $\theta = 0°$, almost the entire LL $N = 1$ and a part of LL $N = 2$ are observed, as explained in Fig. 2(b). The deep dips located near $B_F(\theta)/B = 0.5$ (1.5) correspond to the energy gaps between $N = 0$ (1) and $N = 1$ (2), which is consistent with the Berry phase of π [53,54]. Considering the similarity to the low-field AFM phase, the weak dips located at $B_F(\theta)/B = 1$ and 2 (denoted by red arrows in the schematic diagram) should originate from the spin splitting in the LLs $N = 1$ and 2, respectively. In addition to these splittings, clear dip structures are also discernible around $B_F(\theta)/B = 0.75$ and 1.25 in the LL $N = 1$ (denoted by blue arrows), which suggests the presence of splitting other than the spin origin. As θ increases, the SdH oscillation shows a very complicated change, which is quite different from the θ dependence in the low-field AFM phase. While no significant changes are observed up to $\theta = 15°$, gap collapse is discernible around $B_F/B = 0.75$ and 1.5 at $\theta = 20°$. In particular, the gap collapse at $B_F/B = 1.5$ appears to result from the LL splitting of $N = 2$ (blue arrow), followed by the gap growing above $\theta = 35°$. On the other hand, the gap that collapses at $B_F/B = 0.75$ gradually grows up to 45°. Above $\theta = 50°$, fine split structures become less visible, where the superposition of multiple oscillations varies as a function of θ in a complex manner. Thus the observed θ dependence cannot be explained by simple spin splitting.

For the undoped sample, the θ dependence of SdH oscillation in the high-field AFM phase, which corresponds to the LLs $N = 2$ and 3, is well explained by the spin splitting up to

$\theta = 70°$. For sample Gd#3, on the other hand, the LL $N = 1$ suffers from splitting other than the spin origin, leading to the complicated θ dependence probably due to the overlap with each splitting. Considering four equivalent valleys in the Fermi surface for EuMnBi$_2$ [28], the most plausible origin of the new splitting is the valley splitting [60]. In fact, it is particularly pronounced in the LL $N = 1$ at high magnetic fields, where strong electron-electron interaction is anticipated. Furthermore, in graphene, the LL splitting associated with the spin-valley degrees of freedom shows similar reentrant behavior at tilted fields, i.e., the energy gap collapses and then grows as E_Z/E_c is increased [40]. As future research, it would be important to compare these results with theoretical calculations that consider the variation of valley splitting as a function of θ and its interaction with the spin splitting.

IV. CONCLUSIONS

We report the overall features of Landau level splitting in Gd-doped EuMnBi$_2$, where the Landau level down to $N = 1$ is clearly observed. In the low-field antiferromagnetic phase, the Landau levels ($N = 3$–5) exhibit spin splitting, from which we have found that the effective g factor is enhanced as the Fermi energy approaches the charge-neutral Dirac point. In the high-field antiferromagnetic phase, the Landau level $N = 1$ shows additional splitting other than the spin origin, implying the lifting of valley degeneracy. The complicated variation of Landau level splitting as a function of tilting the field cannot be reproduced by a simple model considering the Zeeman energy.

[1] L. Šmejkal, T. Jungwirth, and J. Sinova, Phys. Status Solidi RRL **11**, 1700044 (2017).

[2] L. Šmejkal, Y. Mokrousov, B. Yan, and A. H. MacDonald, Nat. Phys. **14**, 242 (2018).

[3] S. Nakatsuji, N. Kiyohara, and T. Higo, Nature (London) **527**, 212 (2015).

[4] A. K. Nayak, J. E. Fischer, Y. Sun, B. Yan, J. Karel, A. C. Komarek, C. Shekhar, N. Kumar, W. Schnelle, J. Kubler, C. Felser, and S. S. P. Parkin, Sci. Adv. **2**, e1501870 (2016).

[5] T. Suzuki, R. Chisnell, A. Devarakonda, Y.-T. Liu, W. Feng, D. Xiao, J. W. Lynn, and J. G. Checkelsky, Nat. Phys. **12**, 1119 (2016).

[6] E. Liu, Y. Sun, N. Kumar, L. Muechler, A. Sun, L. Jiao, S.-Y. Yang, D. Liu, A. Liang, Q. Xu, J. Kroder, V. Süß, H. Borrmann, C. Shekhar, Z. Wang, C. Xi, W. Wang, W. Schnelle, S. Wirth, Y. Chen *et al.*, Nat. Phys. **14**, 1125 (2018).

[7] M. Ikhlas, T. Tomita, T. Koretsune, M. Suzuki, D. Nishio-Hamane, R. Arita, Y. Otani, and S. Nakatsuji, Nat. Phys. **13**, 1085 (2017).

[8] A. Sakai, Y. P. Mizuta, A. A. Nugroho, R. Sihombing, T. Koretsune, M. Suzuki, N. Takemori, R. Ishii, D. Nishio-Hamane, R. Arita, P. Goswami, and S. Nakatsuji, Nat. Phys. **14**, 1119 (2018).

[9] K. Sumida, Y. Sakuraba, K. Masuda, T. Kono, M. Kakoki, K. Goto, W. Zhou, K. Miyamoto, Y. Miura, T. Okuda, and A. Kimura, Commun. Mater. **1**, 89 (2020).

[10] X. Li, L. Xu, L. Ding, J. Wang, M. Shen, X. Lu, Z. Zhu, and K. Behnia, Phys. Rev. Lett. **119**, 056601 (2017).

[11] C. Wuttke, F. Caglieris, S. Sykora, F. Scaravaggi, A. U. B. Wolter, K. Manna, V. Süß, C. Shekhar, C. Felser, B. Büchner, and C. Hess, Phys. Rev. B **100**, 085111 (2019).

[12] S. N. Guin, K. Manna, J. Noky, S. N. Guin, K. Manna, J. Noky, S. J. Watzman, C. Fu, N. Kumar, W. Schnelle, C. Shekhar, Y. Sun, J. Gooth, and C. Felser, NPG Asia Mater. **11**, 16 (2019).

[13] T. Higo, H. Man, D. B. Gopman, L. Wu, T. Koretsune, O. M. J. van't Erve, Y. P. Kabanov, D. Rees, Y. Li, M. Suzuki, S. Patankar, M. Ikhlas, C. L. Chien, R. Arita, R. D. Shull, J. Orenstein, and S. Nakatsuji, Nat. Photonics **12**, 73 (2018).

[14] Y. Okamura, S. Minami, Y. Kato, Y. Fujishiro, Y. Kaneko, J. Ikeda, J. Muramoto, R. Kaneko, K. Ueda, V. Kocsis, N. Kanazawa, Y. Taguchi, T. Koretsune, K. Fujiwara, A. Tsukazaki, R. Arita, Y. Tokura, and Y. Takahashi, Nat. Commun. **11**, 4619 (2020).

[15] J. Park, G. Lee, F. Wolff-Fabris, Y. Y. Koh, M. J. Eom, Y. K. Kim, M. A. Farhan, Y. J. Jo, C. Kim, J. H. Shim, and J. S. Kim, Phys. Rev. Lett. **107**, 126402 (2011).

[16] J. K. Wang, L. L. Zhao, Q. Yin, G. Kotliar, M. S. Kim, M. C. Aronson, and E. Morosan, Phys. Rev. B **84**, 064428 (2011).

[17] K. Wang, D. Graf, H. Lei, S. W. Tozer, and C. Petrovic, Phys. Rev. B **84**, 220401(R) (2011).

[18] K. Wang, D. Graf, L. Wang, H. Lei, S. W. Tozer, and C. Petrovic, Phys. Rev. B **85**, 041101(R) (2012).

[19] J. B. He, Y. Fu, L. X. Zhao, H. Liang, D. Chen, Y. M. Leng, X. M. Wang, J. Li, S. Zhang, M. Q. Xue, C. H. Li, P. Zhang, Z. A. Ren, and G. F. Chen, Phys. Rev. B **95**, 045128 (2017).

[20] Y. Feng, Z. Wang, C. Chen, Y. Shi, Z. Xie, H. Yi, A. Liang, S. He, J. He, Y. Peng, X. Liu, Y. Liu, L. Zhao, G. Liu, X. Dong, J. Zhang, C. Chen, Z. Xu, X. Dai, Z. Fang *et al.*, Sci. Rep. **4**, 5385 (2014).

[21] L.-L. Jia, Z.-H. Liu, Y.-P. Cai, T. Qian, X.-P. Wang, H. Miao, P. Richard, Y.-G. Zhao, Y. Li, D.-M. Wang, J.-B. He, M. Shi, G.-F. Chen, H. Ding, and S.-C. Wang, Phys. Rev. B **90**, 035133 (2014).

[22] L. Li, K. Wang, D. Graf, L. Wang, A. Wang, and C. Petrovic, Phys. Rev. B **93**, 115141 (2016).

[23] Y. Y. Wang, Q. H. Yu, and T. L. Xia, Chin. Phys. B **25**, 107503 (2016).

[24] M. Kondo, M. Ochi, T. Kojima, R. Kurihara, D. Sekine, M. Matsubara, A. Miyake, M. Tokunaga, K. Kuroki, H. Murakawa, N. Hanasaki, and H. Sakai, Commun. Mater. **2**, 49 (2021).

[25] A. F. May, M. A. McGuire, and B. C. Sales, Phys. Rev. B **90**, 075109 (2014).

[26] H. Masuda, H. Sakai, M. Tokunaga, Y. Yamasaki, A. Miyake, J. Shiogai, S. Nakamura, S. Awaji, A. Tsukazaki, H. Nakao, Y. Murakami, T. Arima, Y. Tokura, and S. Ishiwata, Sci. Adv. **2**, e1501117 (2016).

[27] A. Wang, I. Zaliznyak, W. Ren, L. Wu, D. Graf, V. O. Garlea, J. B. Warren, E. Bozin, Y. Zhu, and C. Petrovic, Phys. Rev. B **94**, 165161 (2016).

[28] S. Borisenko, D. Evtushinsky, Q. Gibson, A. Yaresko, K. Koepernik, T. Kim, M. N. Ali, J. van den Brink, M. Hoesch, A. Fedorov, E. Haubold, I. Kushnirenko, I. Soldatov, R. Schäfer, and R. J. Cava, Nat. Commun. **10**, 3424 (2019).

[29] R. Kealhofer, S. Jang, S. M. Griffin, C. John, K. A. Benavides, S. Doyle, T. Helm, P. J. W. Moll, J. B. Neaton, J. Y. Chan, J. D. Denlinger, and J. G. Analytis, Phys. Rev. B **97**, 045109 (2018).

[30] J. Liu, J. Hu, H. Cao, Y. Zhu, A. Chuang, D. Graf, D. J. Adams, S. M. A. Radmanesh, L. Spinu, I. Chiorescu, and Z. Mao, Sci. Rep. **6**, 30525 (2015).

[31] S. Huang, J. Kim, W. A. Shelton, E. W. Plummer, and R. Jin, Proc. Natl. Acad. Sci. USA **114**, 6256 (2017).

[32] H. Sakai, H. Fujimura, S. Sakuragi, M. Ochi, R. Kurihara, A. Miyake, M. Tokunaga, T. Kojima, D. Hashizume, T. Muro, K. Kuroda, T. Kondo, T. Kida, M. Hagiwara, K. Kuroki, M. Kondo, K. Tsuruda, H. Murakawa, and N. Hanasaki, Phys. Rev. B **101**, 081104(R) (2020).

[33] J. Y. Liu, J. Yu, J. L. Ning, H. M. Yi, L. Miao, L. J. Min, Y. F. Zhao, W. Ning, K. A. Lopez, Y. L. Zhu, T. Pillsbury, Y. B. Zhang, Y. Wang, J. Hu, H. B. Cao, B. C. Chakoumakos, F. Balakirev, F. Weickert, M. Jaime, Y. Lai *et al.*, Nat. Commun. **12**, 4062 (2021).

[34] G. Lee, M. A. Farhan, J. S. Kim, and J. H. Shim, Phys. Rev. B **87**, 245104 (2013).

[35] H. Sakai, J. Phys. Soc. Jpn. **91**, 101001 (2022).

[36] H. Masuda, H. Sakai, M. Tokunaga, M. Ochi, H. Takahashi, K. Akiba, A. Miyake, K. Kuroki, Y. Tokura, and S. Ishiwata, Phys. Rev. B **98**, 161108(R) (2018).

[37] K. Tsuruda, K. Nakagawa, M. Ochi, K. Kuroki, M. Tokunaga, H. Murakawa, N. Hanasaki, and H. Sakai, Adv. Funct. Mater. **31**, 2102275 (2021).

[38] Y. Zhang, Z. Jiang, J. P. Small, M. S. Purewal, Y.-W. Tan, M. Fazlollahi, J. D. Chudow, J. A. Jaszczak, H. L. Stormer, and P. Kim, Phys. Rev. Lett. **96**, 136806 (2006).

[39] Z. Jiang, Y. Zhang, H. L. Stormer, and P. Kim, Phys. Rev. Lett. **99**, 106802 (2007).

[40] A. F. Young, C. R. Dean, L. Wang, H. Ren, P. Cadden-Zimansky, K. Watanabe, T. Taniguchi, J. Hone, K. L. Shepard, and P. Kim, Nat. Phys. **8**, 550 (2012).

[41] S. Awaji, K. Watanabe, H. Oguro, H. Miyazaki, S. Hanai, T. Tosaka, and S. Ioka, Supercond. Sci. Technol. **30**, 065001 (2017).

[42] H. Masuda, H. Sakai, H. Takahashi, Y. Yamasaki, A. Nakao, T. Moyoshi, H. Nakao, Y. Murakami, T. Arima, and S. Ishiwata, Phys. Rev. B **101**, 174411 (2020).

[43] F. Zhu, X. Wang, M. Meven, J. Song, T. Mueller, C. Yi, W. Ji, Y. Shi, J. Ma, K. Schmalzl, W. F. Schmidt, Y. Su, and T. Brückel, Phys. Rev. Res. **2**, 043100 (2020).

[44] We adopted $-d^2\sigma_{xx}/dB^2$ only in the high-field region [at $1/B \leqslant 0.09$ (T^{-1})] to make the oscillatory component clearer; the oscillatory component of $-d^2\sigma_{xx}/dB^2$ is smoothly connected to the oscillatory component of $-d^2\sigma_{xx}/d(1/B)^2$ at $1/B \geqslant 0.09$ (T^{-1}).

[45] F. F. Fang and P. J. Stiles, Phys. Rev. **174**, 823 (1968).

[46] K. Vakili, Y. P. Shkolnikov, E. Tutuc, E. P. De Poortere, and M. Shayegan, Phys. Rev. Lett. **92**, 226401 (2004).

[47] A. Tsukazaki, A. Ohtomo, M. Kawasaki, S. Akasaka, H. Yuji, K. Tamura, K. Nakahara, T. Tanabe, A. Kamisawa, T. Gokmen, J. Shabani, and M. Shayegan, Phys. Rev. B **78**, 233308 (2008).

[48] K. S. Novoselov, A. K. Geim, S. V. Morozov, D. Jiang, M. I. Katsnelson, I. V. Grigorieva, S. V. Dubonos, and A. A. Firsov, Nature (London) **438**, 197 (2005).

[49] Y. Zhang, Y. W. Tan, H. L. Stormer, and P. Kim, Nature (London) **438**, 201 (2005).

[50] See Supplemental Material at http://link.aps.org/supplemental/10.1103/PhysRevB.108.115142 for details of the quantum oscillation for (Eu,Gd)MnBi$_2$ and the calculated results for spin-split Landau levels, which also includes Ref. [36].

[51] T. Osada, J. Phys. Soc. Jpn. **80**, 033708 (2011).

[52] I. A. Luk'yanchuk and Y. Kopelevich, Phys. Rev. Lett. **97**, 256801 (2006).

[53] G. P. Mikitik and Y. V. Sharlai, Phys. Rev. Lett. **82**, 2147 (1999).

[54] Y. Zheng and T. Ando, Phys. Rev. B **65**, 245420 (2002).

[55] For the undoped sample, m_c/m_0 is reported to be 0.122(2) from the temperature dependence of the SdH oscillation [36].

[56] Y. Fuseya, Z. Zhu, B. Fauque, W. Kang, B. Lenoir, and K. Behnia, Phys. Rev. Lett. **115**, 216401 (2015).

[57] M. Komada, H. Murakawa, M. S. Bahramy, T. Kida, K. Yokoi, Y. Narumi, K. Kindo, M. Hagiwara, H. Sakai, and N. Hanasaki, Phys. Rev. B **101**, 045135 (2020).

[58] Z. J. Xiang, D. Zhao, Z. Jin, C. Shang, L. K. Ma, G. J. Ye, B. Lei, T. Wu, Z. C. Xia, and X. H. Chen, Phys. Rev. Lett. **115**, 226401 (2015).

[59] J. Cao, S. Liang, C. Zhang, Y. Liu, J. Huang, Z. Jin, Z. G. Chen, Z. Wang, Q. Wang, J. Zhao, S. Li, X. Dai, J. Zou, Z. Xia, L. Li, and F. Xiu, Nat. Commun. **6**, 7779 (2015).

[60] Y. J. Jo, J. Park, G. Lee, M. J. Eom, E. S. Choi, J. H. Shim, W. Kang, and J. S. Kim, Phys. Rev. Lett. **113**, 156602 (2014).